EBioMedicine 39 (2019) 132–144

Contents lists available at ScienceDirect

EBioMedicine

journal homepage: www.ebiomedicine.com

EBioMedicine
Published by THE LANCET

Research paper

Concomitant type I IFN and M-CSF signaling reprograms monocyte differentiation and drives pro-tumoral arginase production

Yuanyuan Tong [a,1], Luyang Zhou [b,1], Limin Yang [a], Panpan Guo [a], Yanlan Cao [a], F. Xiao-Feng Qin [c], Jianghuai Liu [a,*]

[a] State Key Laboratory of Pharmaceutical Biotechnology and MOE Key Laboratory of Model Animals for Disease Study, Model Animal Research Center of Nanjing University, Nanjing 210061, China
[b] Department of Anesthesiology, Nanjing Gulou Hospital, Affiliated Hospital of Nanjing University Medical School, Nanjing 210008, China
[c] Center of Systems Medicine, Institute of Basic Medical Sciences, Chinese Academy of Medical Sciences and Peking Union Medical College, Beijing 100005, China; Suzhou Institute of Systems Medicine, Suzhou, Jiangsu 215123, China

ARTICLE INFO

Article history:
Received 21 June 2018
Received in revised form 19 November 2018
Accepted 28 November 2018
Available online 7 December 2018

Keywords:
Type I IFN
M-CSF
Arginase
Monocyte maturation
Tumor-associated macrophages
Anti-tumor immunity

ABSTRACT

Background: Type I IFN-based therapies against solid malignancies have yielded only limited success. How IFN affects tumor-associated macrophage (TAM) compartment to impact the therapeutic outcomes are not well understood.
Methods: The effect of an IFN-inducer poly(I:C) on tumor-infiltrating monocytes and TAMs were analyzed using a transplantable mouse tumor model (LLC). *In vitro* culture systems were utilized to study the direct actions by poly(I:C)-IFN on differentiating monocytes.
Results: We found that poly(I:C)-induced IFN targets Ly6C$^+$ monocytes and impedes their transition into TAMs. Such an effect involves miR-155-mediated suppression of M-CSF receptor expression, contributing to restricting tumor growth. Remarkably, further analyses of gene expression profile of IFN-treated differentiating monocytes reveal a strong induction of *Arg1* (encoding arginase-1) in addition to other classical IFN targets. Mechanistically, the unexpected *Arg1* arm of IFN action is mediated by a prolonged STAT3 signaling in monocytes, in conjunction with elevated macrophage colony-stimulating factor (M-CSF) signaling. Functionally, induction of ARG1 limited the therapeutic effect of IFN, as inhibition of arginase activity could strongly synergize with poly(I:C) to enhance CD8$^+$ T cell responses to thwart tumor growth in mice.
Conclusions: Taken together, we have uncovered two functionally opposing actions by IFN on the TAM compartment. Our work provides significant new insights on IFN-mediated immunoregulation that may have implications in cancer therapies.

1. Introduction

Type I IFNs (IFN-Is) are a family of closely related cytokines produced by the innate immune system in response to specific pathogen- or danger-associated molecular patterns [1]. They function *via* a common, broadly expressed IFN-I receptor to activate Jak1/Tyk2, which in turn drive signal transduction mainly *via* the STAT1/STAT2/IRF9 complex called ISGF3. ISGF3 acts as a transcription factor to induce a number of interferon-stimulated genes (ISGs) that mediate IFN-I's potent antiviral, anti-proliferative and immunomodulatory functions [2,3].

The antitumor activities by IFN-Is have long been recognized and are mediated by both tumor-intrinsic and -extrinsic mechanisms [4,5]. Importantly, in defending against solid tumors, IFN-I-mediated enhancements of the innate, as well as the adaptive arms of antitumor immunity are essential [6]. In humans, IFN-I therapies are approved for treatment of several types of cancers [6,7]. More recently, IFN-I-inducing pattern recognition receptor agonists used in either standalone or combinatorial regimens have also shown promising results in cancer clinical trials [8,9]. Additionally, in response to conventional and new generations of therapies, the endogenous IFN-Is produced in the tumor microenvironment are shown to represent key determinants of treatment outcomes [7,10]. Nevertheless, data have also emerged that IFN-I can have tumor-promoting roles under certain contexts [11,12]. In addition, effective cancer treatments by IFN-I or IFN-I-inducers are often limited by systemic toxicities [6]. Such problems may have arisen from the complexities of tumor-associated immune cell types, whose varied responses to IFN-I may not become integrated optimally.

Tumor-associated macrophages (TAMs) are abundant in solid tumors [13]. They play key roles in promoting angiogenesis, tumor growth and metastasis, and in suppressing adaptive antitumor immunity. Their abundance has been generally correlated to poor prognosis of cancer

* Corresponding author.
E-mail address: liujianghuai@nju.edu.cn (J. Liu).
[1] Y.T. and L.Z. contributed equally to this work.

https://doi.org/10.1016/j.ebiom.2018.11.062

Research in context

Evidence before this study

Type I IFN (IFN-I) has been used for treatment of solid malignancies since 1980s. Despite the initial high expectations, IFN-I-based treatment strategies have shown only sub-optimal therapeutic effects. Some evidence has emerged that IFN-I can have complex roles in the tumor microenvironment, limiting its effectiveness in stimulation of anti-tumor immunity.

Added value of this study

Using a preclinical mouse model, this study focused on the impact of poly(I:C)-induced IFN-I on tumor-associated monocytes/macrophages, major constituents of the tumor microenvironment. An miR-155-mediated anti-tumoral pathway as well as an IFN-arginase (ARG1) pro-tumoral axis are identified. The latter pathway also requires the concomitant M-CSF signaling in differentiating monocytes. Inhibition of the newly discovered IFN-ARG1 axis (or related regulatory pathways) can significantly improve the anti-tumor effects by poly(I:C), where notable enhancement of $CD8^+$ T cell responses in tumors were observed.

Implications of all the available evidence

We therefore propose the IFN-ARG1 immunosuppressive axis as a critical "checkpoint" mechanism limiting the efficacies of IFN-I-based therapies, particularly in many tumors that produce high levels of M-CSF. Inhibition of such immunosuppressive axis shall be considered in the future to combine with IFN-I-based therapies. In a broader perspective, it is tempting to suggest that integration of signaling by IFN-I and cues within tumor microenvironment plays a key role in regulating the immunosuppressive functions of monocytes/macrophages. Future investigations in this regard may suggest novel strategies that better harness IFN-I-mediated immunoregulation for treatment of cancers.

patients [14]. The phenotypic and functional features of TAMs are rather diverse in different tumors or even within the same tumors, consistent with the tremendous plasticity of macrophages corresponding to changing environments [15]. Furthermore, besides macrophages, the tumors also contain circulation-borne monocytes that are not only the major precursors to TAMs, but are themselves highly responsive to cues within the tumor microenvironments [16]. The remarkable heterogeneity within this lineage compartment also presents a significant challenge to cancer treatments where tumor-associated monocytes/macrophages have been shown to play complex yet influential roles in determining the therapeutic outcomes in different models [13,14].

Despite strong clinical relevance, the impacts of IFN-I-based therapies on the behaviors of tumor-associated monocytes/macrophages are not fully understood. Although a previous report showed that systemic administration of TLR3 agonist poly(I:C) could directly cause TAMs to undergo tumoricidal, M1-type polarization in a mouse model [17], potential impacts of IFN-I signaling on the TAM compartment was not investigated. In this report, we revealed that the M-CSF-dependent, tumor-associated differentiating monocytes respond to poly(I:C)-induced IFN with a strong up-regulation of arginase-1, which subsequently blunts the cytokine's anti-tumor actions. Our work therefore shed some light on the undesirable tumor-promoting mechanisms associated with IFN-I-based therapies.

2. Materials and methods

2.1. Ethics statement

The animal experiments were approved by the Institutional Animal Care and Use Committee of Nanjing Biomedical Research Institute (NIBR)-NJU. Human PBMCs were obtained from healthy volunteers with informed consent at Nanjing Drum-Tower hospital, where the study was approved by the local ethics committee.

2.2. Reagents

Unless otherwise indicated, all chemicals were purchased from Sigma Aldrich or Sangon. Polyinosinic–polycytidylic acid (poly(I:C)) was purchased from InvivoGen. Mouse IFNβ (#12405–1) and human IFNα were from PBL and Sangon, respectively. The ELISA kits for mIFN-α and mIFNβ were purchased from PBL (#42120–1) and Biolegend (#439407), respectively. The ELISA kit for mM-CSF was purchased from R&D (#MMC00). JAK Inhibitor I (#420099) was from Merck Millipore. The STAT3 inhibitor Stattic (#S7024) and CSF1R inhibitor GW2580 (#S8042) were from Selleckchem. The CCR2 antagonist RS504393 was purchased from Tocris Bioscience (#2517). Cycloheximide (#239763) was from Calbiochem. Human (#300–25) and murine (#315–02) M-CSF were from PeproTech. Arginase inhibitor nor-NOHA (#10006861) was from Cayman.

Primary antibodies for Western blot were purchased from Cell Signaling Technology (Erk1/2, #4695; pErk1/2, #4370; CSF1R, #3152; Stat3, #9139; pStat3-Y705, #9145; arginase-1, #93668; pStat1-Y701, #7649; Stat1, #14994), Santa Cruz (GAPDH, #sc-32,233), BD (ARG1, 610,708, for immunofluorescent staining), Genscript (Actin, #A00730) and Sango (Stat1, #AB55186).

2.3. Methods

2.3.1. Mouse tumor model.

The mice (C57/BL6, 6–8 weeks) were housed and experimented in NIBR-NJU's AAALAC accredited facility (SPF). For tumor induction, 1×10^6 cells of murine Lewis lung carcinoma (LLC) cells were injected subcutaneously (s.c.) into the flank region. Treatments generally started on day 6 after tumor implantation (tumor volumes at ~ 45 mm^3) and lasted for 8 days. Poly(I:C) (7.5 mg/kg, i.p.) was administered every two days while Nor-NOHA (40 mg/kg, i.p.) or CCR2 antagonist (RS504393, 2 mg/kg, i.p.) was introduced daily. GW2580 was administered *via* drinking water (40 mg/kg).

2.3.2. Flow cytometry analyses.

To analyze the stromal immune cells, tumors (6/group) were cut/mixed and digested with trypsin-EDTA (0.05%) at 37 °C for 10 min. The dispersed cells were collected after passing the suspension through a 100-μm nylon mesh. The mouse splenocytes were prepared by mashing the spleen using two frosted ends of glass slides. For analyzing cultured cells, the adherent cells were dissociated from culture plates using 5 mM EDTA and were combined with the non-adherent portions. To analyze the intracellular CSF1R, the cells were fixed at room temperature (R.T., 20 min) using 2% PFA in PBS and then permeabilized for 15 min at R.T. using 0.7% Tween-20 in PBS. The prepared cells were then stained with relevant antibodies (Ly6C, #128022; Ly6G, #127614; CD11b, #101228; F4/80, #123131 & #123122; CD45, #103106 & #103116; CD16/32, #101330 (for FC block); CD3, #100311(Biolegend); and/or CSF1R, #17–1152-82; CD8, #12–0081-82 (eBiosceince)). Cells were analyzed using a BD LSRFortessa platform (or sometimes using a FACSCalibur).

2.3.3. Differentiation of mononuclear cells and purified monocytes.

The mouse bone marrow (BM) mononuclear cells or human PBMCs were prepared using Histopaque-1077 (Sigma). In some cases, the Monocyte isolation kit (BM) from Miltenyi Biotec was used to purify

BM monocytes. The precursor cells were induced for differentiation toward macrophages using M-CSF. The supernatant from minced LLC tumors was also used in some experiments to drive macrophage differentiation [18]. Briefly, the tumors (n = 6, day-10 after inoculation) were cut into small pieces and then homogenized in 5 ml RPMI1640/g tumor tissues. After centrifugation and filtration (0.45 μm), the supernatants of minced tumors were obtained. In some occasions, the levels of M-CSF or type I IFNs within the supernatants were determined using ELISA kits according to manufacturer's instructions. Otherwise, the above supernatants were mixed with basic culture medium 1:1 and fed to mouse BM mononuclear cells.

2.3.4. Gene expression by quantitative real-time PCR.
RNA preparation and qPCR were performed as previously described [19]. The real-time PCR was performed on ABI Step One Plus using gene-specific primers (Supplemental Table 1–1, 1–2). The results were normalized to housekeeping gene GAPDH and HPRT. The quantification of mature microRNAs was also carried out using established protocols [20]. Briefly, total RNA was first polyadenylated. After extraction, the samples were reverse-transcribed using a universal adaptor-adding primer (5′-GCTGTCAACGATACGCTACGTAACGGCATGACAGTGTTTTTTTTTTTTTTTTTTTTC-3′). Consequently, a same reverse primer sequence was used for quantitation of all microRNAs (5′-GCTGTCAACGATACGCTACG-3′). All forward primer sequences are shown in Supplemental Table 1–3. The microRNA expression levels were normalized to those of 5S rRNA and U6 snRNA.

2.3.5. Microarray analysis.
The MACS-purified mouse BM monocytes from a cohort of 12 mice divided into two triplicated groups and treated with M-CSF (20 ng/ml) without or with IFNβ (100 U/ml) for 60 h. The samples were probed against Agilent SurePrint G3 Mouse Gene Expression Microarray 8x60K and data were analyzed *via* R/bioconductor. The raw and processed data were deposited at GEO (GSE115392) and can be openly accessed.

2.3.6. Culture of primary cells and cell lines.
The primary mouse macrophages and fibroblasts were cultured as described [21]. The cell lines (LLC, Raw264.7, 293T and L929) were all from American Type Culture Collection and cultured according to recommended conditions. Lipofectamine 3000 (Invitrogen) was used for transfection of Raw264.7 cells, 293T or BM mononuclear cells. The miR-155 mimic, chemically modified miR-155 inhibitor and the negative control oligos (Genomeditech) (Supplemental Table 1–4) were transfected at a final concentration of 40 nM. For transfection of BM mononuclear cells, the freshly harvested cells were cultured in medium containing M-CSF for 2 h and then were transfected with 25 nM of oligos.

2.3.7. Luciferase reporter assay.
The full-length 3′UTRs of mouse *Csf1r* (NCBI accession, NM_001037859) and Pu.1 (NCBI accession, NM_011355) was amplified from cDNA from macrophages and cloned into the *Xba*I site of pGL3 3′-UTR reporter vector using homologous recombination kit (Vazyme #C112–02). The reporter constructs were used to transfect 293T cells together with either the miR-155 mimic or the control oligo. After 24 h, the cells were harvested and the lysates were analyzed using the Dual-Luciferase Reporter Assay System (Promega).

2.3.8. Immunostaining and histology. Tissue processing and immunofluorescence staining were performed as previously described [21]. Briefly, fixed tumor tissues were embedded in Tissue-Tek OCT compound. The sections (6-μm) were incubated with fluorophore-conjugated primary antibodies or unconjugated primary antibodies (ARG1 (BD); F4/80 (Biolegend)). When necessary, further staining with secondary antibodies (Invitrogen) was applied. The images were taken using an Olympus FV1000 confocal microscope. When the cultured monocytes/macrophages were study subjects, the cells were cytospun onto slides. After fixation in methanol for 5 min, the slides were either subjected to immunofluorescence or H&E staining.

2.3.9. Sorting of monocytes and macrophages using flow cytometry.
FACS sorting was performed on BD FACSAria III high speed sorter. For cell sorting from tumors, the single cell suspensions of tumors (n = 6, day-14 after inoculation) were prepared as described earlier. The following populations were collected: $CD45^+CD11b^+Ly6G^-Ly6C^+F4/80^-$ (monocytes) and $CD45^+CD11b^+Ly6G^-Ly6C^-F4/80^+$ (macrophages). For cell sorting from differentiated monocytes *in vitro*, after 3 days treatment with M-CSF ± IFNβ (100 U/ml), the following populations were collected: $Ly6C^+F4/80^-$ (monocytes) and $F4/80^+$ (macrophages).

2.4. Statistical analysis

All data presented in this study are derived from at least two independent experiments. The effects of treatments on tumor growth were presented as the average measurements (±SD) from at least 6 tumors. Cell abundances determined by flow cytometry are quantified using samples from independent experiments. Cytokine levels were measured by ELISA using prepared supernatants from three individual tumors. Cell counting were presented as average values (±SEM) from at least three random microscopic fields. Levels of protein bands of interest in comparison to a loading control have been determined by densitometry and average values (± variances) from independent experiments are presented. As in standard practices, qPCRs or reporter assays were initially measured using four or three technical replicates. Nevertheless, the presentation of essential results from these quantitative assays reflect biological, but not technical replicates. When applicable throughout the study, Student *t*-tests were performed between given sample groups to determine the P values. If not specifically indicated, asterisks were used to mark the P values in graphs (N.S.: not significant, *: $P < 0.05$, **: $P < 0.01$, ***: $P < 0.001$, ****: $P < 0.0001$, *****: $P < 0.00001$, ******: $P < 0.000001$).

3. Results

3.1. IFN-I targets $Ly6C^+$ monocytes to inhibit monocyte-to-TAM differentiation

Intraperitoneal (i.p.) administration of TLR3 agonist poly(I:C) induces IFN-I/cytokine release, resulting in an apparent systemic IFN response [22]. Previously, such treatment was shown to elicit antitumor effects attributable to several IFN-dependent or -independent mechanisms of immune activation [23]. However, the relevant roles by IFN signaling in tumor-associated monocyte/macrophage compartment had not been clearly characterized. To this end, a transplantable mouse tumor model (LLC) with well-known presence of a significant macrophage compartment was chosen [24]. When introduced i.p., poly(I:C) caused notable inhibition of tumor growth throughout the course of the treatment (Figs. 1A and S1A). The tumor samples harvested at the last time point from the poly(I:C) group showed induction of an interferon-stimulated gene (ISG), *i.e. Isg15*, validating the engagement of an IFN response in tumors (Fig. S1B). Consistent with previous observations [17], a number of M1-type, pro-inflammatory markers were also found to be up-regulated in tumors of the poly(I:C) group. Interestingly, the mRNA levels of a macrophage-selective marker F4/80 (encoded by *Emr1*) showed consistent decrease in the poly(I:C) group (Fig. S1B), suggestive of a decrease in the numbers of tumor-associated macrophages (TAMs). Immunofluorescent microscopy of tumor sections further confirmed such a finding (Fig. 1B, C). It is of note that such intriguing observations on decrease of TAM numbers by the treatment of TLR3 agonist were not previously reported.

As TAMs are largely derived from circulating $Ly6C^+$ monocytes that subsequently infiltrate the tumors [13], we extended our analyses to the overall myeloid populations within tumors, including the monocyte

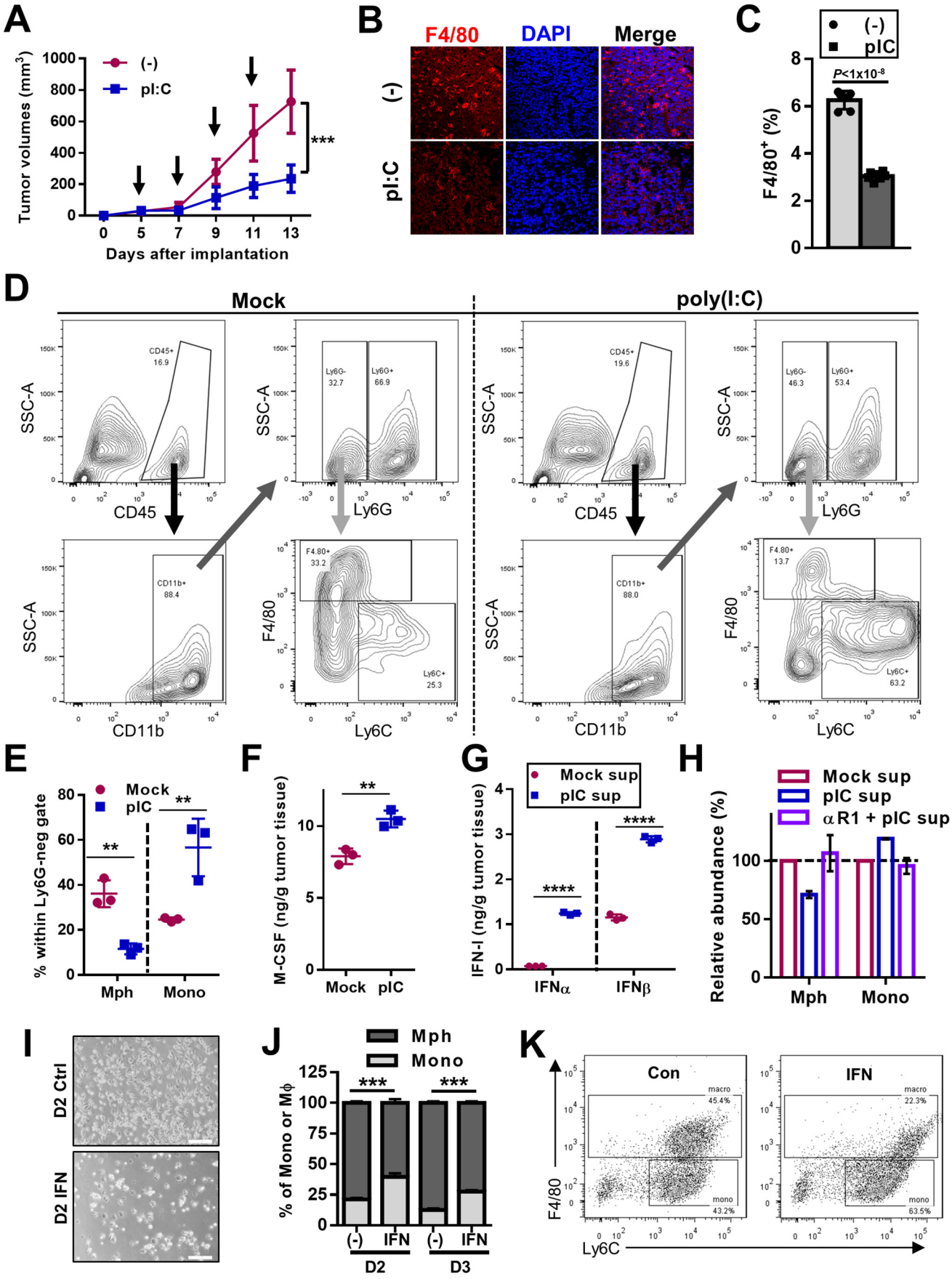
A
Tumor volumes (mm3)
(-)
pI:C
***
Days after implantation
B
F4/80
DAPI
Merge
(-)
pI:C
C
(-)
pIC
P<1x10-8
F4/80+ (%)
D
Mock
poly(I:C)
CD45+ 16.9
Ly6G- 32.7
Ly6G+ 66.9
CD11b+ 88.4
F4.80+ 33.2
Ly6C+ 25.3
CD45+ 19.6
Ly6G- 46.3
Ly6G+ 53.4
CD11b+ 88.0
F4.80+ 13.7
Ly6C+ 63.2
SSC-A
CD45
Ly6G
CD11b
F4/80
Ly6C
E
Mock
pIC
% within Ly6G-neg gate
Mph
Mono
F
M-CSF (ng/g tumor tissue)
Mock
pIC
G
Mock sup
pIC sup
IFN-I (ng/g tumor tissue)
IFNα
IFNβ
H
Mock sup
pIC sup
αR1 + pIC sup
Relative abundance (%)
Mph
Mono
I
D2 Ctrl
D2 IFN
J
Mph
Mono
% of Mono or Mϕ
(-)
IFN
D2
D3
K
Con
IFN
macro 45.4%
mono 43.2%
macro 22.3%
mono 63.5%
F4/80
Ly6C

compartment. When the tumor-associated myeloid cells were selected under the sequential $CD45^+$ and $CD11b^+$ gates, we could then separately examine the numbers of $Ly6G^+$ granulocytic lineage cells as well as the $Ly6G^-$ population that contains both the $F4/80^+$ macrophages and $Ly6C^+$ monocytes [25]. The numbers of $Ly6G^+$ cells were not significantly affected by poly(I:C) in tumors (Fig. S1C, right). Further analyses of the $Ly6G^-$ population in tumors revealed an expected decrease of $F4/80^+$ macrophages (Fig. 1D). In an apparent reverse pattern, the $Ly6C^+$ monocyte subset showed marked increase in the poly(I:C) group (Figs. 1D, E and S1C). In the spleen from the same mice, there were apparent increases in both $Ly6G^+$ cells and $Ly6C^+$ monocytes (Fig. S1C, left), consistent with expansion of such myeloid-derived suppressor cells (MDSC)-like cells by CpG (another IFN inducer) observed previously [26]. The apparent expansion of splenic $Ly6C^+$ monocytes and the evident decrease in tumor macrophage/monocyte ratios collectively suggested that poly(I:C) treatment substantially reduced monocyte-to-TAM conversion.

We next tried to establish an *in vitro* culture system to model the dynamics of monocyte-to-macrophage transition in the control and poly (I:C) group of tumors. M-CSF/M-CSF receptor (CSF1R) is the main ligand/receptor system that drives macrophage lineage commitment and terminal differentiation [27,28]. Indeed, when the mononuclear cells harvested from the BM of naïve mice were cultured in the presence of recombinant M-CSF for two days, a major cell population labeled positively with the macrophage marker F4/80 emerges, accompanying a decrease in their $Ly6C^+F4/80^-$ monocyte precursors (Fig. S1D) [29]. To examine the monocyte differentiation cues within the tumor microenvironment, we prepared the supernatant fractions from minced tumors tissues. Such fractions were found to contain high levels of M-CSF (Fig. 1F), consistent with others' observations with the LLC cell line [30]. The control tumor supernatant sufficed to drive the appearance of a $F4/80^+$ population from BM mononuclear cells in 48 h. The $F4/80^+$ and $Ly6C^+F4/80^-$ populations can also be grossly distinguished by their relative levels of forward scatter (FSC) and side scatter (SSC) (Fig. S1E, right), confirming their respective macrophage and monocyte identities [31]. Moreover, a specific inhibitor against CSF1R tyrosine kinase (GW2580) [32] substantially reduced tumor supernatant-induced conversion of $Ly6C^+F4/80^-$ monocytes into $F4/80^+$ macrophages (Fig. S1E, left).. These results established M-CSF as a major monocyte maturation signal within the LLC tumors.

Compared to the control group, the poly(I:C) group of tumor supernatants drove the conversion of fewer $Ly6C^+F4/80^-$ monocyte precursors into $F4/80^+$ cells (Fig. S1F). Although the latter $F4/80^+$ cells appeared to express higher levels of Ly6C, the size and granularity of the cells validated their macrophage identities. Therefore, our observations *in vivo* (Fig. 1D) are recapitulated by *in vitro* examinations of tumor supernatant-dependent monocyte differentiation, suggesting that soluble cues within the tumor microenvironment are responsible for poly(I:C)-dependent inhibition of monocyte-to-TAM differentiation. Since the levels of M-CSF in tumors from poly(I:C)-treated mice were higher (Fig. 1F), poly(I:C) might have engaged inhibitory signals against monocyte maturation. We tested the contribution by IFN-Is, as the latter were previously shown to inhibit monocyte-to-macrophage differentiation [33]. Expectedly, the levels of both IFNα and IFNβ were significantly elevated in the poly(I:C) group of tumor supernatant (Fig. 1G). Moreover, when the neutralizing antibody against IFN-I receptor (IFNAR1) was added together with poly(I:C) group of tumor supernatant to BM mononuclear cells, the percentages of macrophages and monocytes in the culture (48 h) were normalized to levels achieved by the control supernatant (Figs. 1H and S1G). The antibody also normalized Ly6C levels in macrophages (Fig. S1H), consistent with a role of IFN in up-regulating Ly6C [34].

We next examined the direct effect of IFN-I on differentiation of MACS-purified mouse BM $Ly6C^+F4/80^-$ monocytes (Fig. S1I). Judged by the criteria of plate-adherences (Fig. 1I), morphology (Figs. 1J, S1J) and immunophenotypes (Figs. 1K, S1K), we firmly established that IFN-I can directly act on $Ly6C^+$ monocytes to impede monocyte-to-macrophage transition. It is important to note that, when IFN was added to BM cells that had been previously differentiated under M-CSF for 3 days, no subsequent decrease in adherent cells were observed (data not shown), arguing against a potential role of IFN on mature macrophage survival. Similar to the situation in mouse cells, IFN also inhibited the differentiation of human PBMCs toward macrophages, as judged by cells' plate-adherences (Fig. S1L) and down-regulation of macrophage markers (Fig. S1M, N). Taken together, our *in vivo* and *in vitro* observations strongly suggest that systemic poly(I:C)-induced IFN-I can target tumor-associated monocytes to inhibit their M-CSF-dependent transition into TAMs.

3.2. IFN inhibits the expression of CSF1R protein in differentiating monocytes and macrophages

Although similar inhibitory effects by IFN-I on monocyte maturation had been noted previously [33,35], the underlying mechanisms were not understood. ERK1/2 signaling plays an essential role on CSF1R-dependent macrophage differentiation [27]. Indeed, time-dependent increases in ERK1/2 phosphorylation were observed in M-CSF-driven, mouse differentiating monocytes (Fig. 2A). Notably, we found that these cells had reduced levels of pERK1/2 at 24 h following IFN treatment, which later recovered at 48 h (Fig. 2A). To simplify data interpretations, we treated the terminally differentiated, M-CSF-starved macrophages (BMDMs and peritoneal macrophages (PMs)) with or without IFN for overnight and then stimulated with M-CSF for 10 min. As expected, IFN treatment led to an apparent induction of STAT1, the product of a classical ISG. Importantly, the immediate M-CSF signaling was blunted by IFN (Figs. 2B and S2A). It is worth noting that overnight M-CSF withdraw together with IFN treatment on macrophages did not result in apparent global effects such as notable changes in their numbers or morphologies (data not shown).

To further understand IFN's inhibitory effect on proximal M-CSF signaling, we examined the levels of cell surface CSF1R. During M-CSF-driven monocyte differentiation, cell surface CSF1R levels gradually increased in a population of transitional monocytes (Fig. 2C) [29]. Such increases in CSF1R were apparently suppressed by IFN in time points from 24 h to 72 h. Interestingly, the mRNA levels of *Csf1r* was not reduced significantly within the first 48 h of treatment (Fig. 2D). Since CSF1R is indispensable for M-CSF signaling [27,28], our results therefore strongly suggest that IFN-mediated down-regulation of cell surface CSF1R levels accounts for its inhibitory effect on monocyte-to-macrophage transition.

Fig. 1. IFN-I targets $Ly6C^+$ monocytes to inhibit monocyte-to-TAM differentiation. (A) The mice were injected (s.c.) with 1×10^6 LLC cells in the flanks. Starting on day 5 after tumor implantation, IFN-I-inducer poly(I:C) was administered (i.p.) every two days. The changes in tumor sizes were determined (±SD, n = 6, P value is marked for the last time point). Arrows indicate treatments. (B–E) Tumors were harvested after 4 treatments. (B) Sections were analyzed by F4/80 immunofluorescence microscopy (scale: 50 μm). (C) Quantitation from 6 random fields (±SD) is presented (P value marked). The myeloid compartments in disintegrated tumor tissues (6 combined) were analyzed by FACS (D and E). Representative plots are shown (D). In (E), the mean percentages (±SD) of macrophages (Mph) and monocytes (Mono) are presented (three independent experiments, P values for both subsets marked) (F–H) Tumor-burden mice (day 9) were mock- or poly(I:C)-treated for 12 h and the tumors were harvested. In (F and G), supernatants were prepared from individual minced tumors (n = 3). The levels of M-CSF (F) or IFNα/β (G) in the supernatants were determined by ELISA (±SD, P values marked). In (H), the BM mononuclear cells were fed with the supernatants (sup) from minced tumor tissues (six tumors combined). Control IgG or IFNAR-blocking antibody (10 μg/ml) were included in the medium. In 48 h, cells were FACS-analyzed for Ly6C and F4/80. Average abundance of these subsets (relative) from two independent experiments are presented (± data range). (I-K) MACS-purified monocytes were cultured in 20 ng/ml M-CSF ± IFNβ (100 U/ml). The extents of cells' plate-adherence are shown in (I) (scale: 100 μm). (J) Cells were subjected to cytospin/H&E staining and their constitutions were quantitated (±SEM, three random fields). (I) Cells were also analyzed by FACS after 24 h of treatments.

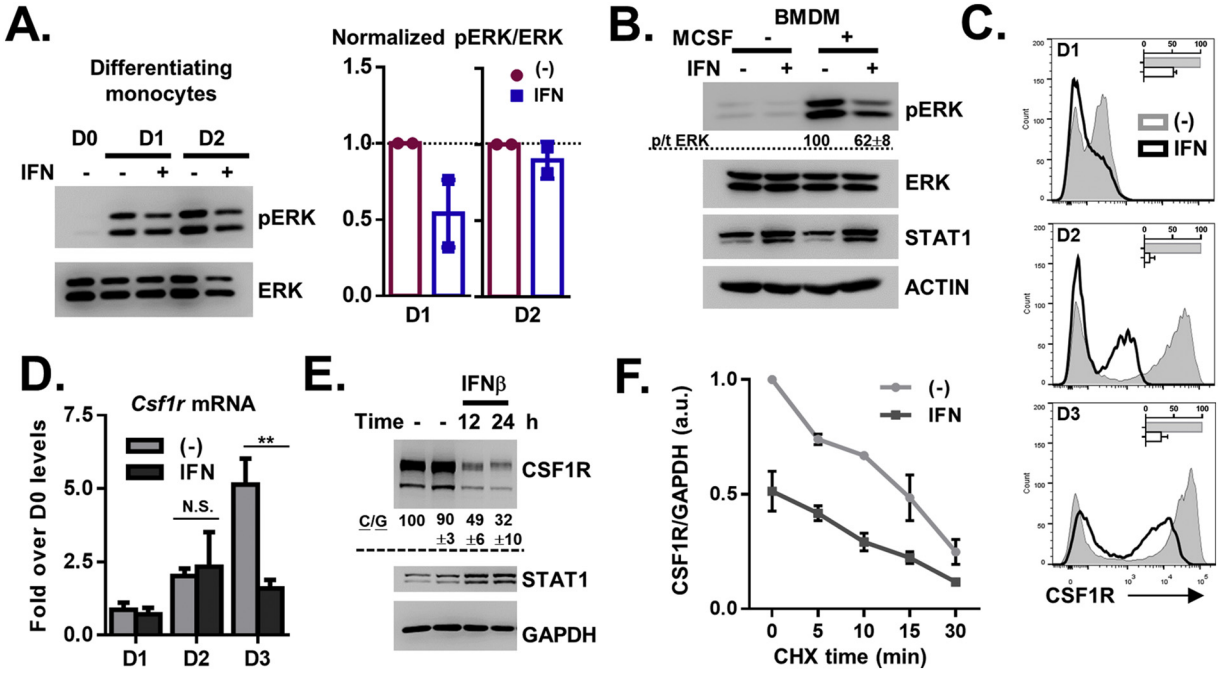

Fig. 2. IFN inhibits the expression of CSF1R protein in differentiating monocytes and macrophages. (A) MACS-purified monocytes were treated with M-CSF ± IFNβ. Protein samples at indicated times were analyzed by Western blot (WB, left). Densitometry analyses for bands of pERK1/2 or total ERK1/2 were performed. The relative ratios pERK/ERK from two independent experiments are presented on the right (mean ± range). (B) The BMDMs were pre-treated with IFNβ (500 U/ml, 12 h) and were next stimulated with M-CSF for 10 min before lysate harvest. After WB, the ratios between pERK and ERK (p/t ERK) were determined. Average values (± data range) from two independent experiments were marked underneath the WB panel of pERK1/2. (C and D) The experiment was performed as in (A). Cell surface CSF1R and *Csf1r* mRNA were analyzed by FACS (C) and qPCR (D) in three independent experiments, respectively. In (C), representative FACS plots are presented. The median fluorescence intensities (MFI) for the $CSF1R^+$ subsets were determined (relative) and the average values (±SEM) are shown in insets of individual FACS plots. In (D), the relative levels of *Csf1r* mRNA (±SEM, P values marked at given time points) are shown. (E) The levels of intracellular CSF1R in IFN-treated BMDMs (500 U/ml) were analyzed by WB. The normalized CSF1R levels were determined (against GAPDH, C/G). Quantifications from two independent experiments (mean ± range) are marked. (F) BMDMs were pre-treated with IFN for 12 h and then CHX (2 μg/ml) was added for indicated time points. After WB, normalized CSF1R levels were determined against GAPDH. Average data (± range) from two independent experiments were presented.

Similar down-regulation of cell surface CSF1R was also observed in IFN-treated mature macrophages and a macrophage cell line, Raw264.7 (Fig. S2B). As expected, the mRNA levels of *Csf1r* in parallelly treated BMDMs and Raw264.7 cells were not affected (Fig. S2C). We further found that IFN-mediated down-regulation of cell surface CSF1R in BMDMs was blunted by pre-treatment of the cells with a selective Jak inhibitor, at a dose resulting in partial inhibition of ISG induction (Fig. S2D, E), establishing the participation of Jak pathway in such an effect.

Using flow cytometry analyses of fixed/permeablized cells (Fig. S2F), as well as Western blotting (Fig. 2E), we further demonstrated down-regulation of total CSF1R protein within 24 h of IFN treatment in BMDMs. To examine the turnover of CSF1R, BMDMs were pre-treated with or without IFN and then added with protein synthesis inhibitor cycloheximide (Fig. 2F and S2G). Consistent with previous findings [36], CSF1R protein showed fast turnover. Nevertheless, its half-life was not further accelerated following IFN treatment. Taken together, our results so far had pointed to a most probable scenario that the inhibitory effect of IFN on CSF1R occurs at the level of mRNA translation.

3.3. IFN induces miR-155 to target the 3′-UTR of Csf1r mRNA

One group of regulators of mRNA translation and/or stability are the miRNAs [37]. Therefore, potential *Csf1r*-targeting miRNAs were predicted using the Targetscan program [38]. When the levels of all high-probability miRNA regulators were examined in monocytes, several of them (miR-155 and miR-449a/b/c) showed apparent decreases upon monocyte maturation (Fig. S3A), implying that their down-regulation may contribute to the concomitant up-regulation of cell surface CSF1R (Fig. 2C). Nevertheless, of all tested miRNAs, only miR-155 was notably induced by IFN in monocytes (Fig. 3A). Similar induction also occurred in IFN-treated human PBMCs (Fig. 3B). Generally consistent with others' findings [39], IFN treatment led to up-regulation of miR-155 in BMDMs and Raw264.7 (Fig. S3B). In stark contrast, no such induction was seen in the non-myeloid MEFs or L929 cells (Fig. S3C). We noted that miR-155 was previously shown to regulate CSF1R [40]. Furthermore, miR-155 was known to regulate some targets mainly at the level of mRNA translation [41,42].

Therefore, we tested the link between miR-155 and CSF1R. Using a luciferase reporter of *Csf1r* 3′-UTR (or a mutant at the miR-155-targeted sequence) (Fig. 3C), together with an miR-155 mimic oligo, we validated that miR-155 predictably targets *Csf1r* mRNA (Fig. 3D). A reporter corresponding to the 3′-UTR of *Spi1* mRNA (encoding PU.1), a known miR-155 target [41], was used as a positive control. Consistently, transfection with an miR-155 inhibitor oligo led to up-regulation of CSF1R in Raw264.7 cells, confirming the contribution of endogenous miR-155 in regulating CSF1R (Fig. 3E). Additionally, transfection of differentiating monocytes with an mir-155 mimic oligo led to reduced monocyte-to-macrophage conversion (Fig. 3F), associated with down-regulation of cell surface CSF1R (Fig. 3G).

Next, we probed the relevance of IFN-mir-155-CSF1R inhibitory circuit in tumor-associated monocytes/macrophages *in vivo*. Indeed, poly(I:C) treatment of LLC tumor-burden mice led to notable up-regulation of miR-155 and down-regulation of CSF1R in whole tumors (Fig. 3H, I). To functionally define the role of IFN-CSF1R inhibitory circuit in tumors, CSF1R inhibitor GW2580 was used together with poly(I:C) in tumor-bearing mice to further impede CSF1R function. As expected, the combinatorial treatment led to additive inhibition of TAM numbers, as well as macrophage marker *Emr1* mRNA (Fig. S3D, E). Furthermore, in general agreements with many other studies of CSF1R targeting (reviewed in [13]), GW2580 enhanced poly(I:C)-mediated control of tumor progression (Fig. 3J), pointing to an anti-tumoral role by the engaged miR-155-CSF1R inhibitory circuit in the monocyte/macrophage compartment.

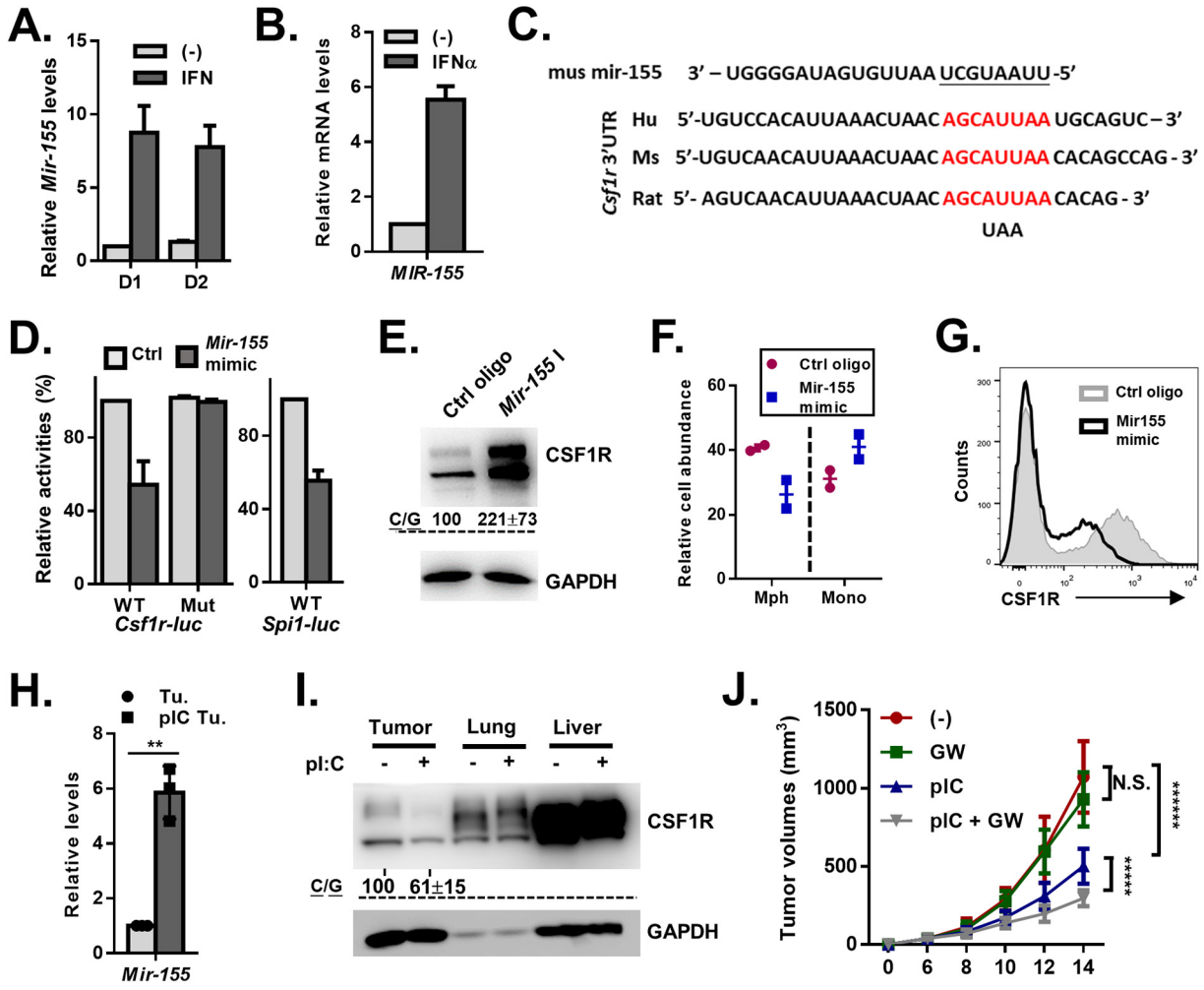

Fig. 3. IFN induces miR-155 to target the 3′-UTR of *Csf1r* mRNA. (A and B) MACS-purified monocytes (A) or human PBMCs (B) were treated with M-CSF ± IFNβ (or IFNα for PBMC) and the relative levels of miR-155 were analyzed (± range, two independent experiments). (C) The potential miR-155-targeted site (red font) in *Csf1r* 3′UTR is conserved. Mutations made to disrupt the targeting by miR-155 was shown underneath. (D) 293T cells were co-transfected with WT (or mutant) *Csf1r* or PU.1 3′ UTR reporter ± miR-155 mimic. Luciferase activities were determined. Data presented are average values (± range) from two independent experiments. (E) Raw264.7 cells were transfected (2 times) ± a miR-155 inhibitor oligo and protein samples were analyzed. Average quantifications (± range) from two independent experiments are marked. (F and G) BM mononuclear cells cultured in M-CSF were transfected with a miR-155 mimic oligo (or a control oligo) in two independent experiments. Three days after transfection, cells were subjected to flow cytometry analyses. In (F), the relative abundance of macrophages ($F4/80^+$) and monocytes ($Ly6C^+F4/80^-$) were determined (± range). In (G), the levels of CSF1R in the transfected differentiating monocytes are shown (representative plots). (H) The levels of miR-155 in control or treated tumor tissues (day 14) from three independent experiments were analyzed (±SD, P value marked). (I) The level of CSF1R protein in tumor tissues, lung tissues and liver tissues from mock- or poly(I:C)-treated mice (day 14) were analyzed by WB. Relative levels in the tumor tissue are marked (mean ± range, n = 2). (J) Tumor-burden mice were treated with or w/o GW2580 (40 mg/kg) in drinking water starting on day 6. Concomitantly, poly(I:C) was administrated as described earlier, either alone or together with GW2580. Tumor sizes were measures throughout the experiment (±SD, n = 12). Student *t*-tests were performed on the values obtained at the end of the experiment (P values between given groups marked).

3.4. IFN-I signaling in differentiating monocytes unexpectedly leads to strong induction of arginase-1

Our results so far revealed that the differentiating $Ly6C^+$ monocytes represent a major IFN-responding cell type within the tumor microenvironment, where the rate of their conversion into TAMs is impeded by IFN. As IFN-I was known to engage diverse, cell type-specific responses [43], we next utilized microarray analyses to examine the functional role of IFN (60 h) on differentiating monocytes (Fig. 4A). Expectedly, many classical ISGs appeared in the up-regulated genes. Gene ontology (GO) analysis revealed that genes whose functions related to interferon response, host defense and immune activation were enriched in the up-regulated gene list (Fig. S4A). Consistently, IFN-mediated induction of some common proinflammatory markers was confirmed by qPCR (Fig. S4B). To our surprise, the gene exhibiting the greatest fold increase by IFN in such a system was *Arg1* (Fig. 4B), encoding arginase-1, whose remarkable induction pattern was confirmed by qPCR (Fig. S4B). Arginase-1 catalyzes a key step in arginine catabolic pathway and is mostly known to play a pro-tumor role in tumor-associated myeloid cells [44]. The extent of *Arg1* induction by IFN in differentiating monocytes greatly exceeded those of several other immunosuppressive genes that previously reported to be IFN-inducible (Fig. S2B) [10]. Furthermore, genes within the GO term of “arginine transport” are enriched within the list of IFN-up-regulated genes from the microarray (Fig. S4A). These striking results implicated that IFN-treated differentiating monocytes indeed also engaged an arginase-dependent pro-tumoral program.

We further confirmed the induction of arginase-1 protein in IFN-stimulated (60 h) differentiating monocytes (Fig. 4C). A marked up-regulation in total STAT1 protein (an ISG) in comparison to its previously noted low baseline level in differentiating monocytes [45] was used as a positive control. Note that at such a late time point, pSTAT1 became difficult to detect and was therefore not used in our studies as controls (Fig. S4C). In the ensuing experiment, it was found that *Arg1*

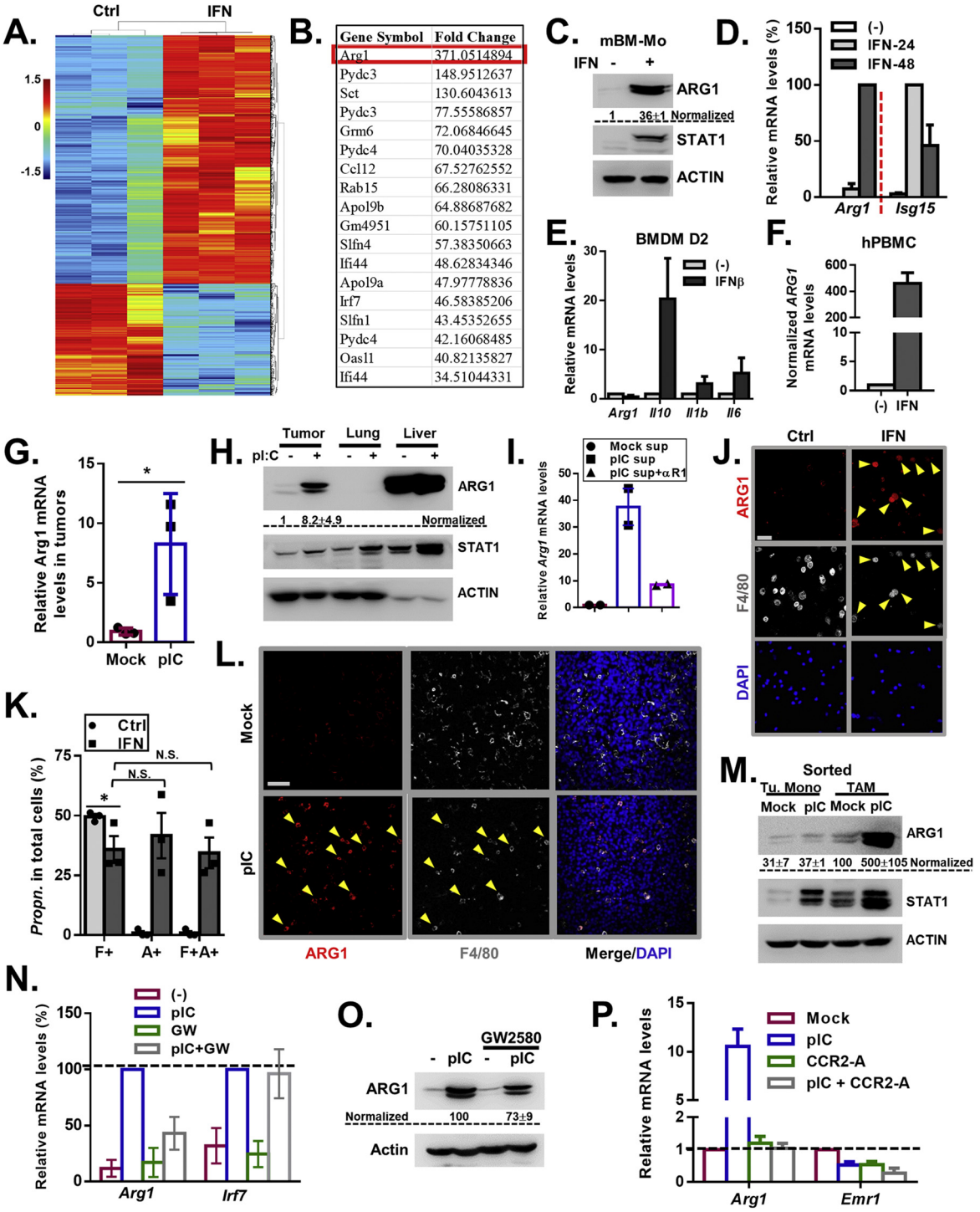

Fig. 4. IFN-I signaling in differentiating monocytes unexpectedly leads to strong induction of arginase-1. (A–C) The MACS-purified BM monocytes were cultured in M-CSF ± IFN for 60 h. Microarray analyses were performed. Heatmap of differentially expressed genes is presented in (A). (B) Genes with the greatest fold-changes are presented (*Arg1* highlighted). (C) Protein samples were analyzed by Western blot (WB). Average quantifications of normalized ARG1 levels (± range) from two independent experiments are marked. (D-F) Mouse BM mononuclear cells (D), mature BMDMs (E) or human PBMCs were treated w/M-CSF ± IFNβ for indicated times (PBMC with IFNα for 5 days). RNA samples were analyzed by qPCR. Average data (± range) from two independent experiments are presented. (G and H) Relative levels of *Arg1* mRNA as normalized to its liver levels (G) or ARG1 protein (H) in control and treated tumors (day 14) are presented. In (G), data were from 3 independent experiments (±SEM, P value marked). In (H), some normal tissue samples were included. Quantifications of normalized tumor ARG1 levels were averaged (± range, n = 2). (I) BM mononuclear cells were cultured within the control or poly(I:C) group of supernatants from minced tumor tissues for 60 h in two independent experiments. The poly(I:C) group was also added with neutralizing antibody against IFN receptor (αR1). The mRNA levels of *Arg1* were determined (± range). (J and K) BM mononuclear cells were cultured in M-CSF ± IFNβ for 60 h. After cytospin, the slides were then co-stained with indicated antibodies for immunofluorescence analyses ((J), scale: 50 μm). Arrowheads point at positively stained cells. In (K), the cells positive for ARG1 (A+), F4/80 (F+) or both markers (F + A+) were quantitated (±SEM, 3 fields, P values between given groups marked). (L and M) In (L), sections of tumors (day 14) were immunostained as in (J). In (M), tumor associated monocytes or macrophages were sorted by flow cytometry in two independent experiments. Samples from sorted cells were subjected to WB analysis. Average quantifications of normalized ARG1 levels are marked (± range). (N and O) Tumor-burden mice were treated ± poly(I:C) ± GW2580 and tumors were harvested (day 14). The samples were subjected to qPCR (N) or WB analyses (O), respectively. Average quantifications from two independent experiments are presented (± range). (P) Tumor-burden mice were treated with ± poly(I:C) ± CCR2 antagonist RS504393 (CCR2-A) on day 6 after tumor implantation. Tumors were harvested on day 14 and subjected to qPCR analyses (± range, n = 2).

induction by IFN was apparently not the consequence of a differentiation block, as the mRNA levels of *Arg1* remain relatively unchanged during monocyte maturation (Fig. S4D). Interestingly, unlike *Isg15*, a classical ISG whose induction peaked around 24 h, *Arg1* mRNA induction by IFN became much more substantial at 48 h (Fig. 4D). Moreover, in contrast to IFN-I, type II IFN used at the same concentration caused minimal up-regulation of *Arg1* (Fig. S4E). Intriguingly, in differentiated bone marrow-derived macrophages (BMDMs) cultured under M-CSF, IFNβ failed to stimulate *Arg1* mRNA (Fig. 4E). Therefore, *Arg1* induction by IFN-I in monocytes is both stimulus- and differentiation stage-restricted. Moreover, we confirmed that in human peripheral blood mononuclear cells (PBMCs) cultured under M-CSF, IFN-I treatment also led to a notable up-regulation of *ARG1* mRNA (Fig. 4F).

Consistent with results from cultured monocytes, increased expression of arginase-1 at both mRNA (~10 fold induction) and protein levels were seen in the whole LLC tumors from poly(I:C)-treated mice, while no such trend was observed in the lungs or livers from the same animals (Fig. 4G, H). The restricted ARG1 induction by poly(I:C)-IFN in tumors is likely to be attributed to their ability to continuously recruit infiltrating monocytes where the IFN-ARG1 axis can be subsequently engaged.

We next used supernatants from minced tumors to examine whether poly(I:C)-stimulated IFN-I in the tumor microenvironment may contribute to inducing *Arg1* expression in differentiating monocytes. Notably, compared to the control group, the poly(I:C) group of supernatant caused a much higher expression of *Arg1* in the BM culture, which could be largely prevented by a neutralizing antibody against IFNAR1 (Fig. 4I and S4F). It is worth noting that direct Poly(I:C) treatment of BM mononuclear cells did not lead to induction of *Ifnb* or *Arg1* mRNAs (Fig. S4G), consistent with their low expression of TLR3 [46]. Moreover, when BMDMs were treated with poly(I:C), *Arg1* mRNA levels were only moderately induced (Fig. S4H, < 5-fold). Since tumor-associated myeloid cells represent a relatively small percentage of the whole tumor mass, such a moderate, direct induction of *Arg1* mRNA is not possible to account for its substantial changes in whole tumors (see Fig. 4G). Therefore, the results from the above *in vitro* characterization experiments strongly support a model that poly(I:C)-induced IFN-I subsequently acts on tumor-infiltrating monocytes, driving marked induction of arginase-1.

During monocyte-to-macrophage differentiation, cells belonging to either stages co-exist. Therefore, we determined the maturation status of the cells expressing high levels of ARG1 following IFN stimulation. Remarkably, in IFN-treated BM mononuclear cells, high levels of ARG1 were mostly localized in the newly formed F4/80$^+$ macrophages (arrowheads, <50% of the total cells) (Fig. 4J, K). Similarly, poly(I:C)-induced ARG1 expression in tumors was largely localized in F4/80$^+$ TAMs (Fig. 4L). Such a macrophage-restricted ARG1 induction in tumors were also corroborated by analysis of *Arg1* mRNA and protein levels in sorted monocytes and macrophages from tumors (Figs. 4M and S4I). Consistent with the restriction of poly(I:C)-dependent ARG1 expression in the TAM compartment, pharmacological depletion of TAMs (see Fig. S3D, E) by CSF1R inhibitor GW2580 led to reduction of *Arg1* mRNA and protein levels in tumors from poly(I:C)-treated mice (Fig. 4N, O). Such an ARG1-reducing effect by GW2580 is likely to contribute to its enhancement of poly(I:C)-mediated antitumor control seen earlier (see Fig. 3J).

Monocyte recruitment to tumors largely involves CCR2 signaling [15]. Therefore, to further support that the infiltrating monocytes in poly(I:C)-treated tumors subsequently differentiate into the ARG1^{high} TAMs, we administered poly(I:C) together with a CCR2 antagonist [47]. Such inhibitor substantially reduced the levels of tumor-associated monocytes in the poly(I:C) group (Fig. S4J). The numbers of TAMs were also reduced, but to a lesser extent, likely attributed to the longer life-spans of macrophages than those of monocytes [48]. Importantly, CCR2 blockade greatly reduced poly(I:C)-mediated *Arg1* mRNA induction in tumors (Fig. 4P), functionally linking monocyte recruitment to subsequent ARG1 induction in TAMs under the context of poly(I:C) stimulation. Consistent with an expected, pro-tumoral role of ARG1 in TAMs, CCR2 antagonist further enhanced poly(I:C)-mediated control of tumor progression (Fig. S4K).

Besides arginase-1, the rate of arginine catabolism are controlled by the levels of transporter CAT2b (*Slc7a2*) and arginase-2 (*Arg2*) [44,49]. Indeed, similar to that of *Arg1*, the mRNA levels of *Arg2* and *Slc7a2* were induced by poly(I:C) in tumors, but not in the lungs or livers (Fig. S4L). In contrast, no changes in these markers were induced by IFN in cultured LLC cells (Fig. S4M). Collectively, our results have unveiled a non-canonical function of IFN-I in tumor-infiltrating monocytes, *i.e.* induction of a group of genes associated with arginine catabolism.

3.5. IFN-ARG1 axis in differentiating monocytes is mediated by sustained STAT3 activation, in conjunction with M-CSF signaling

Besides activating the canonical ISGF3 complex, IFN-I was also known to activate STAT3 in some cell types [2]. Interestingly, STAT3 was previously shown to up-regulate *Arg1* transcription in MDSCs [50]. Consequently, we tested the contribution of STAT3 signaling to the IFN-ARG1 axis in differentiating monocytes. Mature BMDMs were used as a negative control (see Fig. 4E). With 30 min of treatment by IFN, STAT3 was similarly activated in both BM mononuclear cells and BMDMs (Fig. S5A). However, in longer period of treatment (24 or 48 h), only in IFN-treated, differentiating monocytes, pSTAT3 levels were still notably elevated above the control levels (Fig. 5A, B). Based on the established role by a sustained STAT3 activation in driving an anti-inflammatory program [51], it is plausible that such a difference in STAT3 activation dynamics may have underlied the monocyte-to-macrophage transitional phase-specific *Arg1* induction by IFN. In the ensuing validation experiments, we used a specific inhibitor against STAT3, *i.e.* Stattic [52]. Stattic greatly reduced IFN-mediated induction of *Arg1* mRNA and protein, correlating to its abolishment of IFN-dependent increase of pSTAT3 (Fig. 5C, D). In contrast, the induction of *Isg15* was not affected. These results functionally link STAT3 activation to the IFN-ARG1 axis in differentiating monocytes. Moreover, we also examined the dependence of the IFN-miR-155-CSF1R inhibitory axis on STAT3 activity. Interestingly, IFN-mediated induction of miR-155, as well as down-regulation of CSF1R and macrophage marker *Emr1* in the differentiation monocytes were unaffected by Stattic treatment (Figs. 5E, S5B). These results demonstrate that the IFN-ARG1 axis and IFN's inhibition on monocyte maturation can be separated by their different dependence on STAT3.

Since IFN-mediated *Arg1* mRNA induction follows a slow kinetics (Fig. 4D) and the subsequent expression of ARG1 protein appears to be concomitant with M-CSF-driven monocyte-to-macrophage conversion (Fig. 4J), we considered the possibility that M-CSF might serve as a "signal two" to cooperate with IFN in monocytes, driving *Arg1* induction. To test this, IFN was added to monocytes cultured with different concentrations of M-CSF. While such differences in M-CSF dosage did not affect the general IFN responses (Fig. 5F, see *Mx1* levels), the induction of *Arg1* mRNA by IFN was indeed substantiated by increasing concentrations of M-CSF. To analyze the cellular compartment that mainly contribute to the M-CSF-dependent enhancement of *Arg1* expression, we sorted out the monocytes and macrophages from the control or IFN-treated mononuclear cells cultured under different doses (5 or 20 ng/ml) of M-CSF (Fig. S5C). Consistent with the bulk cell analyses (see Fig. 5F), both sorted populations exhibited marked up-regulation of *Mx1*, in a pattern unaffected by the M-CSF concentration (Fig. 5G). Importantly, M-CSF-dependent enhancement of *Arg1* induction by IFN was mostly attributed to the macrophage compartment, where IFN-dependent *Arg1* induction was much more substantial.

As M-CSF also represents a critical survival signal for monocytes *in vitro* [27], it was not feasible to treat monocytes with IFN alone for long term, in the absence of M-CSF. Alternatively, we considered to add IFN to naïve BM mononuclear cells cultured with another myeloid

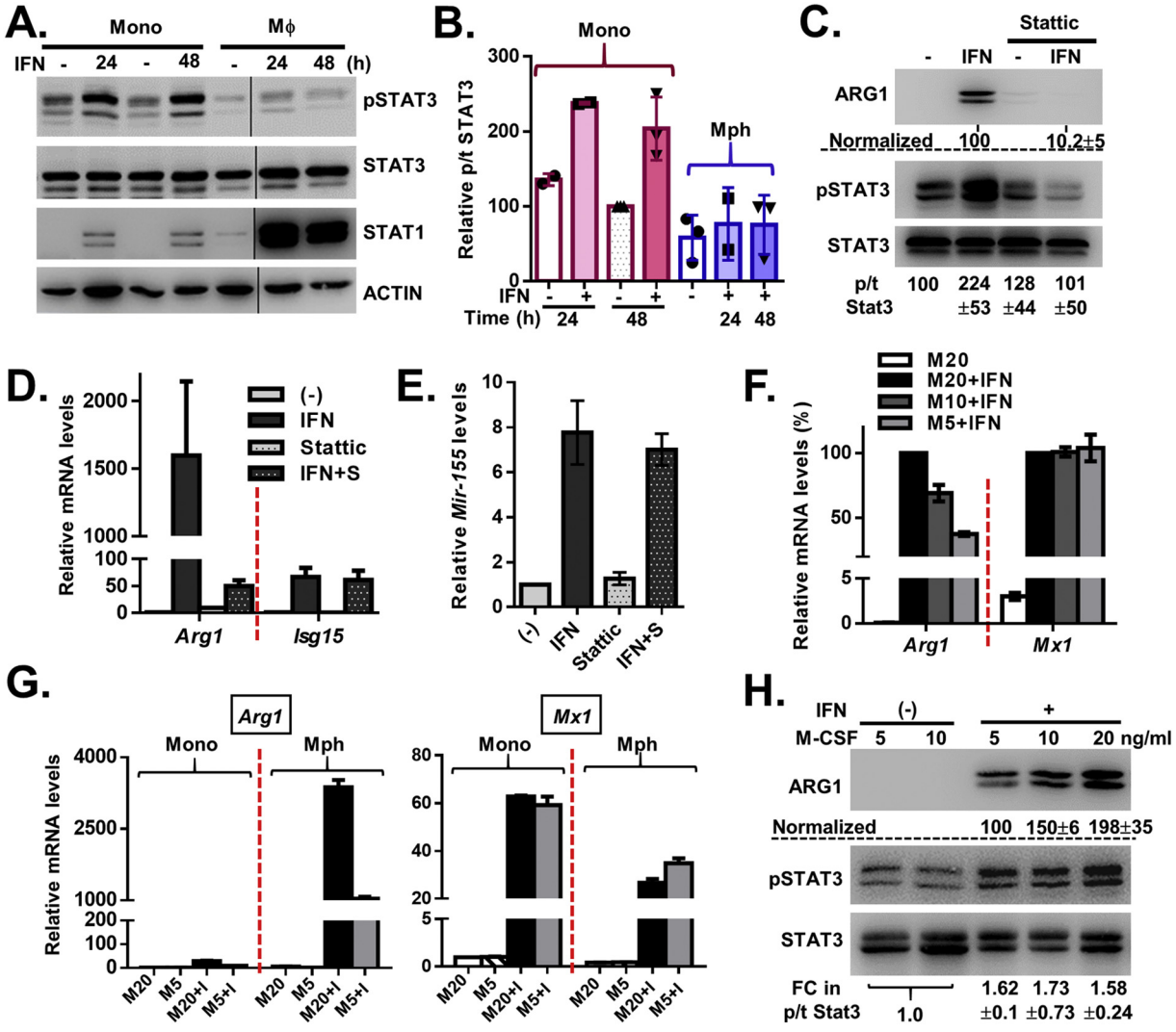

Fig. 5. IFN-ARG1 axis in differentiating monocytes is mediated by sustained STAT3 activation, in conjunction with M-CSF signaling. (A and B) BM mononuclear cells and BMDMs were cultured in M-CSF ± IFNβ for 24 or 48 h, as indicated. Protein samples were analyzed by WB (A). The levels of phosphor/total STAT3 at all time point were quantified and normalized against the levels in control monocyte culture at 48 h (%). Average values (± range) from three independent experiments (two for some time points) are presented (B). (C and D) The BM mononuclear cells were cultured in M-CSF ± IFNβ ± Stattic (5 μM) for 60 h. Protein samples and RNA samples were analyzed by WB (C) and qPCR (D), respectively. Quantifications (± range) from two independent experiments are presented. (E) The BM mononuclear cells were cultured in M-CSF ± IFNβ ± Stattic (5 μM) for 60 h. The relative levels of miR-155 were determined (± range, n = 2). (F to H) BM mononuclear cells were cultured in different concentrations of M-CSF as indicated. RNA samples from unsorted cells were analyzed in (F). The *Arg1* or *Mx1* mRNA from cells treated with IFN together with 20 ng/ml of M-CSF in two independent experiments were set as 100 (%). Average values (± range) are presented. In (G), monocytes and macrophages were first sorted out by flow cytometry and were then harvested for RNA analyses. Protein samples from unsorted cells were analyzed in (H). Quantifications were made from two independent experiments.

growth factor, GM-CSF. We observed high levels of *Arg1* mRNA in GM-CSF-treated cells (Fig. S5D), consistent with a previous work [53]. However, co-addition of IFN to the GM-CSF-present cultures did not further increase *Arg1* mRNA levels, despite that *Isg15* was robustly induced. Taken together, our results show that M-CSF, but not GM-CSF "licenses" IFN-driven *Arg1* induction in monocytes under conversion toward macrophages. Mechanistically, although increasing M-CSF concentrations led to increments in ARG1 expression, the pY705 STAT3 levels were similar among the samples (Fig. 5H), suggesting that M-CSF and IFN signaling interact at nodes beyond STAT3 Y705 phosphorylation.

3.6. Poly(I:C) and arginase inhibitor exhibit synergistic anti-tumor effects in mice

Our work thus far demonstrates that IFN can parallelly drive down-regulation of CSF1R as well as induction of ARG1 in TAMs. Due to the generally considered pro-tumoral role of arginase-1 [44], it stands as another promising TAM-related therapeutic target. We considered to combine poly(I:C) treatment with administration of a commercially available arginase inhibitor, *i.e.* Nor-NOHA [49]. Interestingly, in cultured differentiating monocytes, Nor-NOHA treatment led to near abrogation of IFN-induced *Arg1* mRNA (Fig. 6A), similar to others' observations with the inhibitor [49,54]. As a control, the induction of a classical ISG, *Isg15* was not affected. Since arginase-mediated usage of L-arginine can have a secondary effect on the NOS2-NO axis, an important redox-dependent signaling hub [55,56], our results with Nor-NOHA points to an intriguing possibility that redox signaling might regulate IFN-ARG1 induction.

In tumor-bearing mice, Nor-NOHA alone showed a modest inhibitory effect on tumor growth, consistent with most pre-clinical studies targeting arginases [24,49,57,58]. Nevertheless, Nor-NOHA clearly synergized with poly(I:C) in slowing tumor growth through the course of the treatment (Fig. 6B). As a control, the body weights of mice were not significantly different among experimental groups (Fig. 6C). In resemblance to the pattern of *Arg1* mRNA in cultured monocytes (Fig. 6A), poly(I:C)-induced ARG1 protein in tumors were

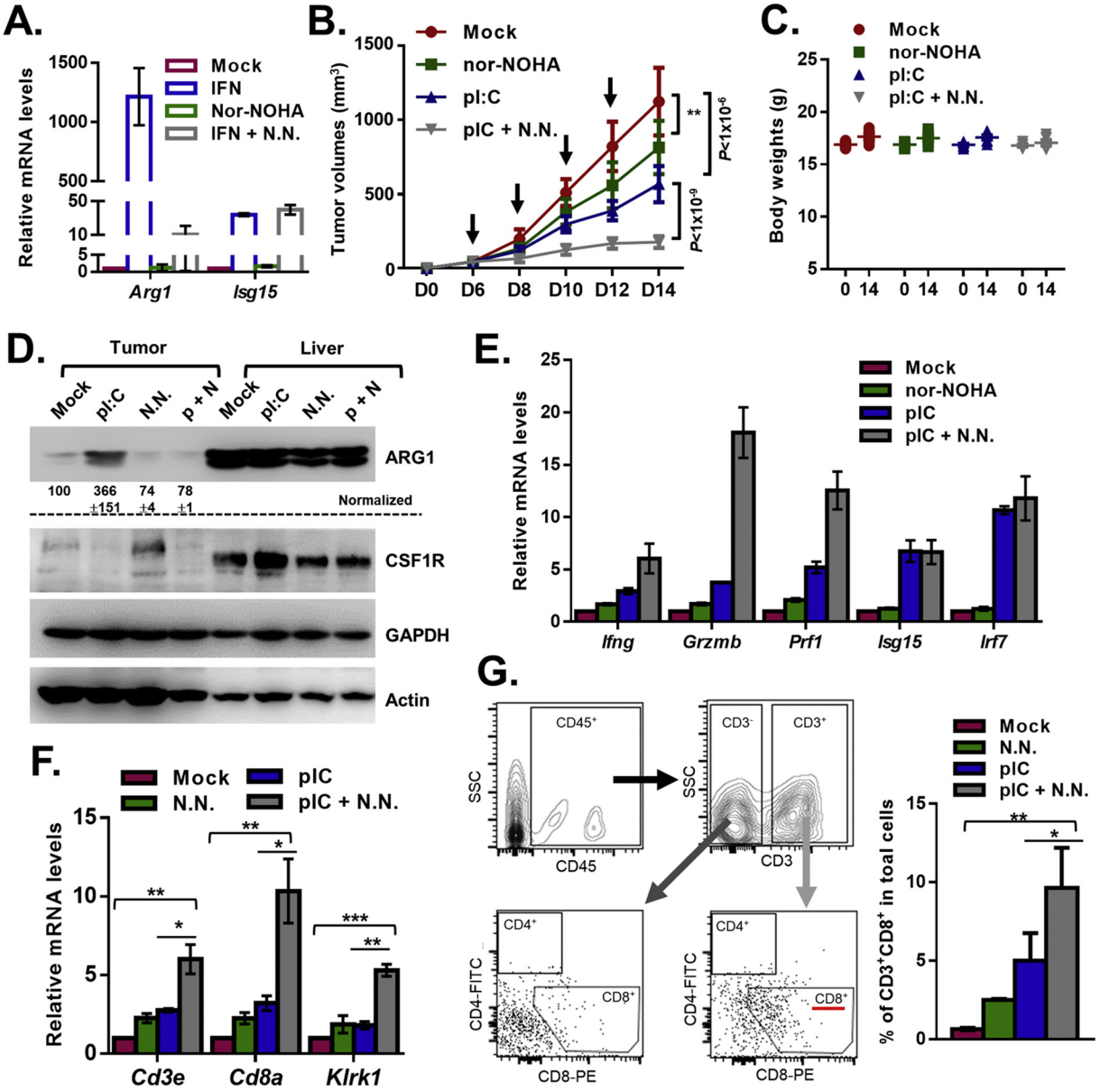

Fig. 6. Poly(I:C) and arginase inhibitor exhibit synergistic anti-tumor effects in mice. (A) BM mononuclear cells were cultured in M-CSF ± IFNβ ± Nor-NOHA (2 mM) for 48 h (two independent experiments). The qPCR data using RNA samples are presented (± range). (B–D) Tumor-burden mice were treated ± poly(I:C) ± Nor-NOHA (40 mg/kg) for 8 days. The tumor volumes (±SD, n = 12, Student *t*-tests done for day 14) (B) and body weights (C) are presented. In (C), there are no statistically significant differences between any treatment groups. Protein samples from tumors and livers were analyzed (D) and quantifications of tumor ARG1 levels are marked (± range, n = 2). (E–G) The experiments were performed as described in (B), except that the tumors were harvested after 3 days of treatment (on day 9). The levels of T cell activation markers (E) or general markers for $CD8^+$ T cells (F) were determined by qPCR. Samples were harvested after treatment of three independent mice cohorts. Average data from two ((E), ± range) or three ((F), ±SEM, P values between given groups marked) independent experiments are presented. In (G), tumor tissue where subjected to flow cytometry using indicated gating strategies (left, plots of mock-treated tumors). The percentages of $CD8^+$ T cells within all cells are presented on the right (±SD, P values between given groups marked).

greatly reduced by Nor-NOHA co-treatment (Fig. 6D). Since arginase activities from TAMs were known to suppress an effective anti-tumor immune response [13], we harvested tumors at an early time point of treatment (day 3 after treatment). Importantly, a group of activation markers for T cells were most strongly up-regulated in the co-administration group (Fig. 6E), whereas induction of an IFN response by poly(I:C) was not further promoted. Furthermore, the mRNA levels of general $CD8^+$ (but not of the $CD4^+$, not shown) T cell markers showed similar trends as the above activation markers, suggesting synergistic increase in tumoricidal T cells (Fig. 6F). Interestingly, as a marker that is shared by natural killer (NK) cells and activated $CD8^+$ T cells [59], the mRNA levels of *Klrk1* (encoding NKG2D) was also highest in the co-treatment group. Nevertheless, a potential involvement of NK cells was not further tested. Additional flow cytometry analyses showed that the numbers of $CD8^+$ T cells in tumors were significantly higher in the co-treatment group (Fig. 6G), whereas the abundance of $CD4^+$ T cells were rather low in all groups. These results suggest that arginase inhibition may potentiate the immune-stimulatory action by poly(I:C), leading to more effective anti-tumor T cell responses.

4. Discussions

IFN-Is have been exploited as anti-cancer drugs in the clinics. Nevertheless, how IFN signaling impacts the monocyte/macrophage lineage compartment to shape an anti-tumor response was not clearly

understood. Based on analyses of a syngeneic mouse tumor model and *in vitro* BM precursor culture systems, the present study first established that poly(I:C)-induced IFN targets Ly6C$^+$ monocytes in tumors to inhibit their maturation toward TAMs (Fig. 1). We next uncovered miR-155-dependent suppression of *Csf1r* mRNA translation as a critical underlying mechanism (Figs. 2, 3). Further *in vitro* and *in vivo* experiments revealed a surprising regulatory axis where IFN-I exposure during this particular monocyte maturation stage leads to a robust induction of arginase-1 in subsequently matured TAMs (Fig. 4). Originally considered as an M2 macrophage marker induced by IL-4/IL-13 in the mouse system, ARG1 is a potent immuno-suppressive enzyme whose expression is now found to be upregulated in different myeloid cells by a variety of stimuli including growth factors, hypoxia and even some pro-inflammatory stimuli [44,60,61]. Interestingly, while IL-4 and IL-13 fail to reproduce the *Arg1*-inducing effect in human PBMCs [61,62], the IFN-*Arg1* axis can be similarly engaged in mouse and human systems (see Fig. 4D and F), implicating the functional significance of such regulation. Although IFN-I is mostly known to be immunostimulatory against tumors, our results suggest an additional theme of regulation that a robust ARG1 up-regulation by IFN in monocytes-derived TAMs may be counter-effective.

Mechanistically, we find that the IFN-ARG1 pathway is most probably mediated by a long-durational STAT3 signaling engaged by IFN selectively in the differentiating monocytes, but not in the mature macrophages (Fig. 5A, B, C, D). Similar distinctions in basal pSTAT3 levels were previously described between MDSCs and TAMs and were attributed to their differences in specific phosphatase activities [63]. Whether such possibility applies to our system warrants future investigations. Nevertheless, our results are consistent with the notion that the functional heterogeneities in macrophages may be attributed to their differences in maturation status and the resulting diversities in cellular responses [61]. Furthermore, the correlation between the sustained STAT3 activation in differentiating monocytes and the relative slow kinetics of *Arg1* induction associated with the maturation progress (Fig. 5A, B and Fig. 4D, J) implies that STAT3 may participate in a multi-dimensional regulatory program, which leads to the eventual, remarkable activation of *Arg1* transcription. In support of such a notion, we found that IFN-mediated ARG1 induction in BM mononuclear cells appeared to also require parallel M-CSF signaling (Figs. 5F, G, H and S5D). Such a "licensing" effect by M-CSF on IFN-ARG1 axis is consistent with this growth factor's known involvement in differentiation/maintenance of macrophages exhibiting M2-like, tolerant phenotypes [28]. As the nature, strength and duration of M-CSF signaling, as well as the associated molecular effects are conceivably different between monocytes that were either undifferentiated or undergoing conversion into macrophages [27], we speculate that such distinctions may be another crucial determinant to further restrict high *Arg1* induction by IFN selectively in newly differentiated macrophages (see Figs. 4J and 5G). To place our data into a broader perspective, we favor a hypothetical, monocyte-centric, "two-signal" model that the integration of signals from the inflammatory mediators (signal 1) and myeloid growth factors (signal 2) in the monocytic precursors critically determines the function of subsequently derived macrophages. As many growing tumors are continuously infiltrated by monocytes [16], further testing the above model and potentially probing the associated mechanistic principles would shed more light on the molecular basis for the ever-elusive natures of TAMs. Regarding the immediate clinical relevance, we suggest that the scenario of IFN-I driving TAM ARG1 expression may particularly operate in many solid tumors that produce high levels of M-CSF [13], subsequently influencing their responses to IFN-I.

Consistent with a pro-tumoral role by the IFN-ARG1 axis in monocytes/TAMs, blockade of CCR2-dependent monocyte recruitment to tumors (Fig. S4K), suppression of CSF1R-mediated monocyte-to-macrophage maturation (Fig. 3J), or inhibition of arginases (Fig. 6B) all led to improvement of poly(I:C)-mediated anti-tumor control. On the practical side, results from our preclinical, co-treatment experiments have pointed to several potential targeting strategies to combine with IFN-I-based therapies or IFN-inducing conventional therapies, especially for tumors highly expressing M-CSF. Focusing on the poly(I:C) and arginase inhibitor co-treatment regimen that was most effective in our study, we observed significantly enhanced CD8$^+$ T cell responses (Fig. 6). Therefore, our work has revealed an IFN-driven, monocyte/macrophage-centered "checkpoint" pathway whose targeting may subsequently lead to unleashing the adaptive anti-tumor immunity. It is worth noting that for all the above mentioned IFN-sensitizing targets (CCR2, CSF1R and ARG1), there are multiple designed drugs in clinical development [28,58,64], making more advanced translational research approachable.

Our study also adds to the evidence that IFN-I can have complex immune-regulatory roles [7]. In contrast to the arginase-inducing aspect discussed above, our initially characterized IFN-miR155-CSF1R inhibitory axis in differentiating monocytes is likely to dampen the signaling *via* the IFN/M-CSF-ARG1 pathway and contribute to IFN's anti-tumoral effect (Figs. 3J and 4N, O). These findings may be helpful for future treatment designs centered on targeting CSF1R. Despite mainly being considered as a TAM-selective drug target, CSF1R in the non-myeloid stromal cells can inadvertently complicate the therapeutic effect by pharmacological CSF1R inhibition [30]. As IFN-I-induction of miR-155 shows monocytes/macrophages-selective pattern (see Figs. 3A, B and S2C), to combine lower dosage CSF1R inhibitors/blockers [28] with IFN-I-based therapies (to induce the miR-155-CSF1R axis) may limit potential on-target, off-monocyte/macrophage activities by CSF1R targeting to favor therapeutic gain.

Collectively, the present study reveals some functionally opposing actions by IFN-I in tumor-associated monocytes/macrophages that significantly shape poly(I:C)-dependent treatment effects. Further characterization of such opposing actions by IFN-I *via* more detailed analyses of individual myeloid subsets shall unveil additional strategies to harness this cytokine's potent immunoregulatory functions for cancer treatments.

Acknowledgements

We thank the NBRI-NJU for excellent mouse services. We acknowledge the Model Animal Research Center core facility and the Collaborative Liver Disease Research Program of NJU Medical School for instrumental support.

Funding sources

This works is supported by a by National Natural Science Foundation of China grants (31771574, 31471313). The funders had no role in study design, data collection/analysis and interpretation of data.

Declaration of interests

The authors declare no competing interests.

Author contributions

Y.T., L.Z., L.Y., P.G. and Y.C. performed experiments. F.Q. and J.L. designed the experiments. Y.T., F.Q. and J.L. wrote and edited the paper.

Appendix A. Supplementary data

Supplementary data to this article can be found online at https://doi.org/10.1016/j.ebiom.2018.11.062.

References

[1] Takeuchi O, Akira S. Pattern recognition receptors and inflammation. Cell 2010;140(6):805–20.

[2] Ivashkiv LB, Donlin LT. Regulation of type I interferon responses. Nat Rev Immunol 2014;14(1):36–49.
[3] Platanias LC. Mechanisms of type-I- and type-II-interferon-mediated signalling. Nat Rev Immunol 2005;5(5):375–86.
[4] Gresser I, Maury C, Brouty-Boye D. Mechanism of the antitumour effect of interferon in mice. Nature 1972;239(5368):167–8.
[5] Dunn GP, Bruce AT, Sheehan KC, et al. A critical function for type I interferons in cancer immunoediting. Nat Immunol 2005;6(7):722–9.
[6] Parker BS, Rautela J, Hertzog PJ. Antitumour actions of interferons: implications for cancer therapy. Nat Rev Cancer 2016;16(3):131–44.
[7] Zitvogel L, Galluzzi L, Kepp O, Smyth MJ, Kroemer G. Type I interferons in anticancer immunity. Nat Rev Immunol 2015;15(7):405–14.
[8] van den Boorn JG, Hartmann G. Turning tumors into vaccines: co-opting the innate immune system. Immunity 2013;39(1):27–37.
[9] Iribarren K, Bloy N, Buque A, et al. Trial watch: Immunostimulation with Toll-like receptor agonists in cancer therapy. Oncoimmunology 2016;5(3) [e1088631].
[10] Minn AJ, Wherry EJ. Combination cancer therapies with immune checkpoint blockade: Convergence on interferon signaling. Cell 2016;165(2):272–5.
[11] Garcia-Diaz A, Shin DS, Moreno BH, et al. Interferon receptor signaling pathways regulating PD-L1 and PD-L2 expression. Cell Rep 2017;19(6):1189–201.
[12] Benci JL, Xu B, Qiu Y, et al. Tumor interferon signaling regulates a multigenic resistance program to immune checkpoint blockade. Cell 2016;167(6):1540–54 [e12].
[13] Mantovani A, Marchesi F, Malesci A, Laghi L, Allavena P. Tumour-associated macrophages as treatment targets in oncology. Nat Rev Clin Oncol 2017;14(7):399–416.
[14] Ruffell B, Coussens LM. Macrophages and therapeutic resistance in cancer. Cancer Cell 2015;27(4):462–72.
[15] Qian BZ, Pollard JW. Macrophage diversity enhances tumor progression and metastasis. Cell 2010;141(1):39–51.
[16] Noy R, Pollard JW. Tumor-associated macrophages: from mechanisms to therapy. Immunity 2014;41(1):49–61.
[17] Shime H, Matsumoto M, Oshiumi H, et al. Toll-like receptor 3 signaling converts tumor-supporting myeloid cells to tumoricidal effectors. Proc Natl Acad Sci U S A 2012;109(6):2066–71.
[18] Liu D, Chang C, Lu N, et al. Comprehensive proteomics analysis reveals metabolic reprogramming of tumor-associated macrophages stimulated by the tumor microenvironment. J Proteome Res 2017;16(1):288–97.
[19] Tong Y, Li F, Lu Y, Cao Y, Gao J, Liu J. Rapamycin-sensitive mTORC1 signaling is involved in physiological primordial follicle activation in mouse ovary. Mol Reprod Dev 2013;80(12):1018–34.
[20] Wang L, Chen X, Zheng Y, et al. MiR-23a inhibits myogenic differentiation through down regulation of fast myosin heavy chain isoforms. Exp Cell Res 2012;318(18):2324–34.
[21] Jiang H, Shi H, Sun M, et al. PFKFB3-driven macrophage glycolytic metabolism is a crucial component of innate antiviral defense. J Immunol 2016;197(7):2880–90.
[22] Rohlmann A, Gotthardt M, Hammer RE, Herz J. Inducible inactivation of hepatic LRP gene by cre-mediated recombination confirms role of LRP in clearance of chylomicron remnants. J Clin Invest 1998;101(3):689–95.
[23] Sharma S, Zhu L, Davoodi M, et al. TLR3 agonists and proinflammatory antitumor activities. Expert Opin Ther Targets 2013;17(5):481–3.
[24] Colegio OR, Chu NQ, Szabo AL, et al. Functional polarization of tumour-associated macrophages by tumour-derived lactic acid. Nature 2014;513(7519):559–63.
[25] Zhu Y, Knolhoff BL, Meyer MA, et al. CSF1/CSF1R blockade reprograms tumor-infiltrating macrophages and improves response to T-cell checkpoint immunotherapy in pancreatic cancer models. Cancer Res 2014;74(18):5057–69.
[26] Zoglmeier C, Bauer H, Norenberg D, et al. CpG blocks immunosuppression by myeloid-derived suppressor cells in tumor-bearing mice. Clin Cancer Res 2011;17(7):1765–75.
[27] Stanley ER, Chitu V. CSF-1 receptor signaling in myeloid cells. Cold Spring Harb Perspect Biol 2014;6(6).
[28] Hume DA, MacDonald KP. Therapeutic applications of macrophage colony-stimulating factor-1 (CSF-1) and antagonists of CSF-1 receptor (CSF-1R) signaling. Blood 2012;119(8):1810–20.
[29] Francke A, Herold J, Weinert S, Strasser RH, Braun-Dullaeus RC. Generation of mature murine monocytes from heterogeneous bone marrow and description of their properties. J Histochem Cytochem 2011;59(9):813–25.
[30] Kumar V, Donthireddy L, Marvel D, et al. Cancer-associated fibroblasts neutralize the anti-tumor effect of CSF1 receptor blockade by inducing PMN-MDSC infiltration of tumors. Cancer Cell 2017;32(5):654–68 [e5].
[31] Daigneault M, Preston JA, Marriott HM, Whyte MK, Dockrell DH. The identification of markers of macrophage differentiation in PMA-stimulated THP-1 cells and monocyte-derived macrophages. PLoS One 2010;5(1):e8668.
[32] Conway JG, McDonald B, Parham J, et al. Inhibition of colony-stimulating-factor-1 signaling in vivo with the orally bioavailable cFMS kinase inhibitor GW2580. Proc Natl Acad Sci U S A 2005;102(44):16078–83.
[33] Lee PY, Li Y, Kumagai Y, et al. Type I interferon modulates monocyte recruitment and maturation in chronic inflammation. Am J Pathol 2009;175(5):2023–33.
[34] Dumont FJ, Coker LZ. Interferon-alpha/beta enhances the expression of Ly-6 antigens on T cells in vivo and in vitro. Eur J Immunol 1986;16(7):735–40.
[35] U'Ren L, Guth A, Kamstock D, Dow S. Type I interferons inhibit the generation of tumor-associated macrophages. Cancer Immunol Immunother 2010;59(4):587–98.
[36] Lee PS, Wang Y, Dominguez MG, et al. The Cbl protooncoprotein stimulates CSF-1 receptor multiubiquitination and endocytosis, and attenuates macrophage proliferation. EMBO J 1999;18(13):3616–28.
[37] Fabian MR, Sonenberg N, Filipowicz W. Regulation of mRNA translation and stability by microRNAs. Annu Rev Biochem 2010;79:351–79.
[38] Agarwal V, Bell GW, Nam JW, Bartel DP. Predicting effective microRNA target sites in mammalian mRNAs. Elife 2015;4.
[39] Forster SC, Tate MD, Hertzog PJ. MicroRNA as type I interferon-regulated transcripts and modulators of the innate immune response. Front Immunol 2015;6:334.
[40] Riepsaame J, van Oudenaren A, den Broeder BJ, van Ijcken WF, Pothof J, Leenen PJ. MicroRNA-mediated down-regulation of M-CSF receptor contributes to maturation of mouse monocyte-derived dendritic cells. Front Immunol 2013;4:353.
[41] Connell RM, Rao DS, Chaudhuri AA, et al. Sustained expression of microRNA-155 in hematopoietic stem cells causes a myeloproliferative disorder. J Exp Med 2008;205(3):585.
[42] Dunand-Sauthier I, Santiago-Raber M-L, Capponi L, et al. Silencing of c-Fos expression by microRNA-155 is critical for dendritic cell maturation and function. Blood 2011;117(17):4490.
[43] Mostafavi S, Yoshida H, Moodley D, et al. Parsing the interferon transcriptional network and its disease associations. Cell 2016;164(3):564–78.
[44] Rodriguez PC, Ochoa AC, Al-Khami AA. Arginine metabolism in myeloid cells shapes innate and adaptive immunity. Front Immunol 2017;8:93.
[45] Coccia EM, Del Russo N, Stellacci E, Testa U, Marziali G, Battistini A. STAT1 activation during monocyte to macrophage maturation: Role of adhesion molecules. Int Immunol 1999;11(7):1075–83.
[46] Larson SR, Atif SM, Gibbings SL, et al. Ly6C(+) monocyte efferocytosis and cross-presentation of cell-associated antigens. Cell Death Differ 2016;23(6):997–1003.
[47] Mirzadegan T, Diehl F, Ebi B, et al. Identification of the binding site for a novel class of CCR2b chemokine receptor antagonists: binding to a common chemokine receptor motif within the helical bundle. J Biol Chem 2000;275(33):25562–71.
[48] Yona S, Kim KW, Wolf Y, et al. Fate mapping reveals origins and dynamics of monocytes and tissue macrophages under homeostasis. Immunity 2013;38(1):79–91.
[49] Rodriguez PC, Quiceno DG, Zabaleta J, et al. Arginase I production in the tumor microenvironment by mature myeloid cells inhibits T-cell receptor expression and antigen-specific T-cell responses. Cancer Res 2004;64(16):5839–49.
[50] Vasquez-Dunddel D, Pan F, Zeng Q, et al. STAT3 regulates arginase-I in myeloid-derived suppressor cells from cancer patients. J Clin Invest 2013;123(4):1580–9.
[51] El Kasmi KC, Holst J, Coffre M, et al. General nature of the STAT3-activated anti-inflammatory response. J Immunol (Baltimore, Md: 1950) 2006;177(11):7880–8.
[52] Schust J, Sperl B, Hollis A, Mayer TU, Berg T. Stattic: A small-molecule inhibitor of STAT3 activation and dimerization. Chem Biol 2006;13(11):1235–42.
[53] Highfill SL, Rodriguez PC, Zhou Q, et al. Bone marrow myeloid-derived suppressor cells (MDSCs) inhibit graft-versus-host disease (GVHD) via an arginase-1-dependent mechanism that is up-regulated by interleukin-13. Blood 2010;116(25):5738–47.
[54] Takahashi N, Ogino K, Takemoto K, et al. Direct inhibition of arginase attenuated airway allergic reactions and inflammation in a Dermatophagoides farinae-induced NC/Nga mouse model. Am J Physiol Lung Cell Mol Physiol 2010;299(1):L17–24.
[55] Mori M, Gotoh T. Regulation of nitric oxide production by arginine metabolic enzymes. Biochem Biophys Res Commun 2000;275(3):715–9.
[56] Thomas DD, Heinecke JL, Ridnour LA, et al. Signaling and stress: The redox landscape in NOS2 biology. Free Radic Biol Med 2015;87:204–25.
[57] Secondini C, Coquoz O, Spagnuolo L, et al. Arginase inhibition suppresses lung metastasis in the 4T1 breast cancer model independently of the immunomodulatory and anti-metastatic effects of VEGFR-2 blockade. Oncoimmunology 2017;6(6):e1316437.
[58] Steggerda SM, Bennett MK, Chen J, et al. Inhibition of arginase by CB-1158 blocks myeloid cell-mediated immune suppression in the tumor microenvironment. J Immunother Cancer 2017;5(1):101.
[59] Raulet DH. Roles of the NKG2D immunoreceptor and its ligands. Nat Rev Immunol 2003;3:781.
[60] Marvel D, Gabrilovich DI. Myeloid-derived suppressor cells in the tumor microenvironment: expect the unexpected. J Clin Invest 2015;125(9):3356–64.
[61] Murray PJ, Allen JE, Biswas SK, et al. Macrophage activation and polarization: Nomenclature and experimental guidelines. Immunity 2014;41(1):14–20.
[62] Raes G, Van den Bergh R, De Baetselier P, et al. Arginase-1 and Ym1 are markers for murine, but not human, alternatively activated myeloid cells. J Immunol 2005;174(11):6561 [author reply -2].
[63] Kumar V, Cheng P, Condamine T, et al. CD45 phosphatase inhibits STAT3 transcription factor activity in myeloid cells and promotes tumor-associated macrophage differentiation. Immunity 2016;44(2):303–15.
[64] Nywening TM, Wang-Gillam A, Sanford DE, et al. Targeting tumour-associated macrophages with CCR2 inhibition in combination with FOLFIRINOX in patients with borderline resectable and locally advanced pancreatic cancer: A single-centre, open-label, dose-finding, non-randomised, phase 1b trial. Lancet Oncol 2016;17(5):651–62.